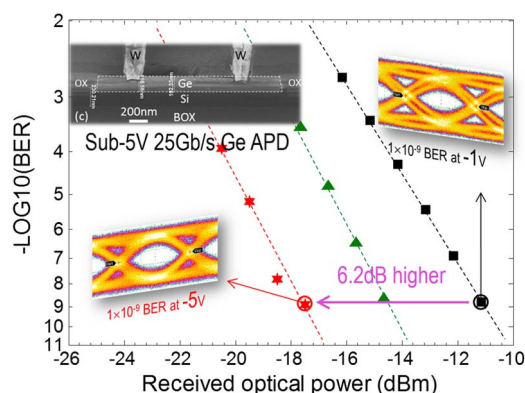


# 25-Gb/s 1310-nm Optical Receiver Based on a Sub-5-V Waveguide-Coupled Germanium Avalanche Photodiode

Volume 7, Number 4, August 2015

H. T. Chen  
J. Verbist  
P. Verheyen  
P. De Heyn  
G. Lepage  
J. De Coster  
P. Absil  
B. Moeneclay  
X. Yin  
J. Bauwelinck  
J. Van Campenhout  
G. Roelkens



DOI: 10.1109/JPHOT.2015.2460116  
1943-0655 © 2015 IEEE

# 25-Gb/s 1310-nm Optical Receiver Based on a Sub-5-V Waveguide-Coupled Germanium Avalanche Photodiode

H. T. Chen,<sup>1,2</sup> J. Verbist,<sup>2,3</sup> P. Verheyen,<sup>1</sup> P. De Heyn,<sup>1</sup> G. Lepage,<sup>1</sup>  
J. De Coster,<sup>1</sup> P. Absil,<sup>1</sup> B. Moeneclaey,<sup>3</sup> X. Yin,<sup>3</sup> J. Bauwelinck,<sup>3</sup>  
J. Van Campenhout,<sup>1</sup> and G. Roelkens<sup>2</sup>

<sup>1</sup>Interuniversity Microelectronics Center (IMEC), 3000 Leuven, Belgium

<sup>2</sup>Photonics Research Group, Department of Information Technology, Ghent University–IMEC,  
9000 Ghent, Belgium

<sup>3</sup>Design Research Group, Department of Information Technology, Ghent University–iMinds–IMEC,  
9000 Ghent, Belgium

DOI: 10.1109/JPHOT.2015.2460116

1943-0655 © 2015 IEEE. Translations and content mining are permitted for academic research only.  
Personal use is also permitted, but republication/redistribution requires IEEE permission.  
See [http://www.ieee.org/publications\\_standards/publications/rights/index.html](http://www.ieee.org/publications_standards/publications/rights/index.html) for more information.

Manuscript received June 24, 2015; revised July 17, 2015; accepted July 19, 2015. Date of publication July 23, 2015; date of current version August 5, 2015. This work was supported in part by the Interuniversity Microelectronics Center (IMEC) industry affiliation program on optical I/O. The transimpedance amplifier (TIA) development was supported by the EU-funded FP7 ICT Projects Mirage, Phoxtrot, and Discus. Corresponding author: H. Chen (e-mail: Hongtao.Chen@imec.be).

**Abstract:** We demonstrate low-voltage waveguide-coupled germanium avalanche photodetectors (APDs) with a (wafer-scale mean) gain $\times$ bandwidth product of 140 GHz at  $-5$  V by utilizing a 185-nm-thick Ge layer. An optical receiver based on such an APD operating up to 25 Gb/s is demonstrated.

**Index Terms:** Avalanche photodetectors (APDs), silicon photonics, optical interconnects.

## 1. Introduction

Avalanche photodetectors (APDs) integrated in a silicon photonics platform offer great potential to improve the link budget of silicon-based optical interconnects by providing significantly improved optical receiver sensitivity as compared to conventional p-i-n photodetectors [1]–[4]. The key design target for CMOS compatible Ge APDs is to obtain low operation voltage. In [5], we demonstrated a 1550 nm 10 Gb/s Si photonics optical receiver based on a waveguide-coupled Ge vertical p-i-n APD. A 5.8 dB sensitivity improvement was obtained at  $-5.9$  V APD bias inferred from bit error ratio measurements.

In this paper, by engineering the Ge APD design, a 10 Gbps 1310 nm optical receiver is demonstrated, showing 7 dB sensitivity improvement at a low APD bias of  $-4.85$  V. A 20 Gbps 1310 nm optical receiver based on such a Ge APD showing 6.2 dB sensitivity improvement at  $-5.0$  V APD bias, and operation of the receiver up to 25 Gbps is demonstrated. A low effective k-value (the ratio of holes impact ionization rate to electrons impact ionization rate) of 0.2 is demonstrated from multiplication noise measurements. The wafer-scale mean gain $\times$ bandwidth product value is 140 GHz at  $-5$  V bias voltage.

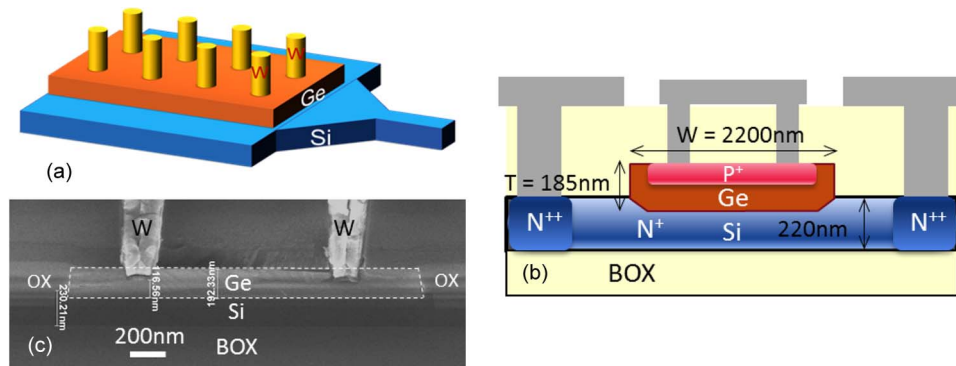


Fig. 1. (a) Schematic of the Ge waveguide APD consisting of the Ge layer and Si waveguide taper. (b) Cross section of the Ge waveguide APD with Ge layer dimensions. (c) SEM cross-section image of the Ge waveguide APD.

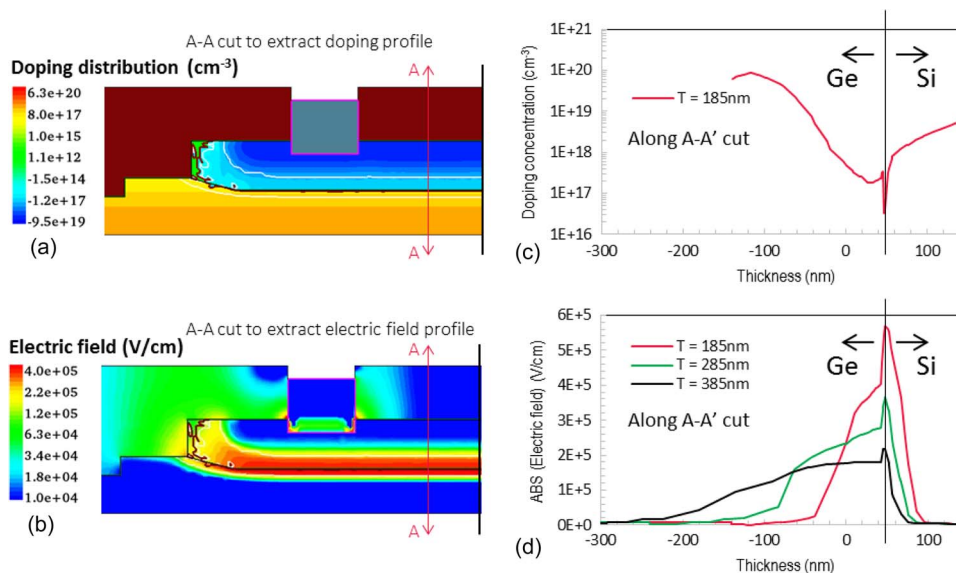


Fig. 2. (a) Simulated doping distribution in the Ge APD. The boron ion implant distribution in the Ge layer was generated from Monte-Carlo simulation. Only half of the structure is shown for clarity. (b) Simulated electric field distribution in the Ge layer at  $-3$  V bias voltage. (c) Doping profile extracted along the A-A' cut [see Fig. 2(a)]. (d) Electric field profiles extracted along the A-A' cut [see Fig. 2(b)] for a Ge layer of 185 nm, 285 nm, and 385 nm in thickness, respectively.

## 2. Device Design and Fabrication

The Ge waveguide APDs were fabricated in imec's fully integrated Si Photonics platform going through a process flow described in [6]. Light is coupled from a 220 nm thick single-mode Si waveguide to the Ge layer using a fully etched waveguide taper, as shown in Fig. 1(a). The Ge layer dimensions and doping configuration are shown in Fig. 1(b). A vertical p-i-n structure (VPIN) is formed by implanting Si with phosphorous ions (before Ge growth) and by implanting the planarized Ge layer with boron ions. The boron ion implant window is uniform in the longitudinal direction. Fig. 1(c) shows a SEM image of the Ge APD cross section.

A 185 nm thin Ge layer was adopted to lower the operation voltage of the Ge APD. The simulated doping distribution in the Ge layer is shown in Fig. 2(a), generated from Monte-Carlo ion implantation simulations calibrated to SIMS data. The doping profile along A-A' [see Fig. 2(a)] is shown in Fig. 2(c). The heterogeneous Ge/Si VPIN configuration together with the 185 nm thin

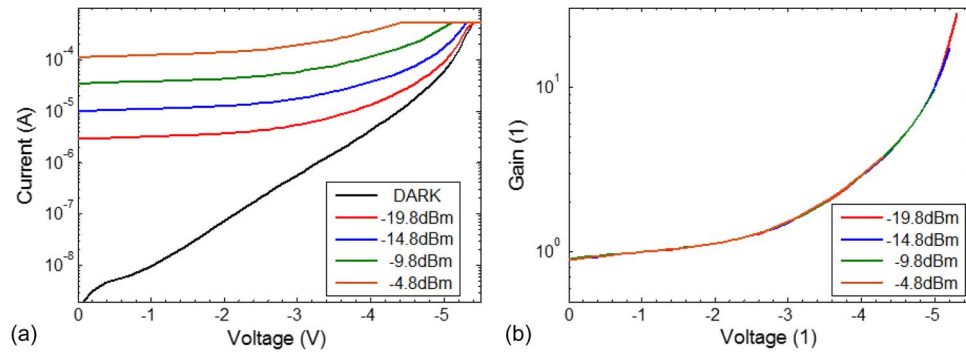


Fig. 3. (a)  $I$ - $V$  characteristics of a  $10\ \mu\text{m}$  long Ge APD device (in the dark and for an input optical power of  $-19.8\ \text{dBm}$ ,  $-14.8\ \text{dBm}$ ,  $-9.8\ \text{dBm}$ , and  $-4.8\ \text{dBm}$ , respectively). (b) Avalanche gain extracted from static measurements under the various input optical powers.

Ge layer results in a strongly non-uniform electric field at  $-3\ \text{V}$  bias voltage, mostly confined in the lower  $100\ \text{nm}$  of the Ge layer, as shown in Fig. 2(b). Fig. 2(d) shows the electric field profile along A-A' [see Fig. 2(b)] for a Ge layer of  $185\ \text{nm}$ ,  $285\ \text{nm}$  and  $385\ \text{nm}$  thick, respectively, at  $-3\ \text{V}$  bias voltage (assuming the same implant conditions). It can be seen that the thinner the Ge layer, the stronger the electric field is in the Ge layer. For the case of a  $185\ \text{nm}$ -thick Ge layer, the electric field strength is calculated to be as high as  $5.2 \times 10^5\ \text{V/cm}$  at the Ge/Si interface at a bias of  $-3\ \text{V}$ . The non-uniform electric field drops sharply to  $1.4 \times 10^5\ \text{V/cm}$  about  $100\ \text{nm}$  away from the interface inside the Ge layer. Therefore, it is expected that strong avalanche multiplication can take place at low bias voltage and that the avalanche excess-noise generation can be suppressed to a great extent due to the limited thickness of the avalanche multiplication region [3], [7]–[9].

### 3. Standalone APD Characteristics

#### 3.1. Static Measurements

Static current-voltage characteristics of a  $10\ \mu\text{m}$  long VPIN Ge APD device are shown in Fig. 3(a). The device has a low dark current of  $\sim 10\ \text{nA}$  at  $-1\ \text{V}$ . The light current was measured at  $1310\ \text{nm}$  wavelength under an waveguide referred input optical power of  $-19.8\ \text{dBm}$ ,  $-14.8\ \text{dBm}$ ,  $-9.8\ \text{dBm}$  and  $-4.8\ \text{dBm}$ , respectively. A compliance current of  $0.5\ \text{mA}$  was applied in the measurements. The measured primary responsivity is  $0.3\ \text{A/W}$  at  $-1\ \text{V}$ . The light current increases rapidly as the bias voltage surpasses  $-3\ \text{V}$ , owing to the adopted thin Ge layer design. The avalanche gain extracted from static measurements is consistent for the various input optical powers, as shown in Fig. 3(b).

As the Ge thickness is merely  $185\ \text{nm}$ , a small variation in this thickness over the wafer could have an impact on the device performance. Therefore wafer scale measurements of the static device performance were carried out. Wafer scale primary responsivity data (in the bottom half of the wafer) of the Ge APD at  $-1\ \text{V}$  under an input optical power of  $-19.8\ \text{dBm}$  are shown in Fig. 4(a). The mean primary responsivity value is  $0.3\ \text{A/W}$  with a standard deviation of  $0.06\ \text{A/W}$ . Fig. 4(b) shows wafer scale avalanche gain data extracted from static measurements at  $-5\ \text{V}$  under an input optical power of  $-19.8\ \text{dBm}$ . The mean avalanche gain value is  $10.6$  with a standard deviation of  $2.4$ . Both the primary responsivity data and avalanche gain data indicate a uniform wafer-scale APD static performance.

#### 3.2. Small-Signal RF Measurements

Next, small-signal radio-frequency (RF) measurements were carried out at  $1310\ \text{nm}$  using an average optical input power of  $-14.2\ \text{dBm}$ . As shown in Fig. 5, with increasing bias voltage, the generated low-frequency RF power increases substantially. Fig. 6(a) shows the wafer-scale

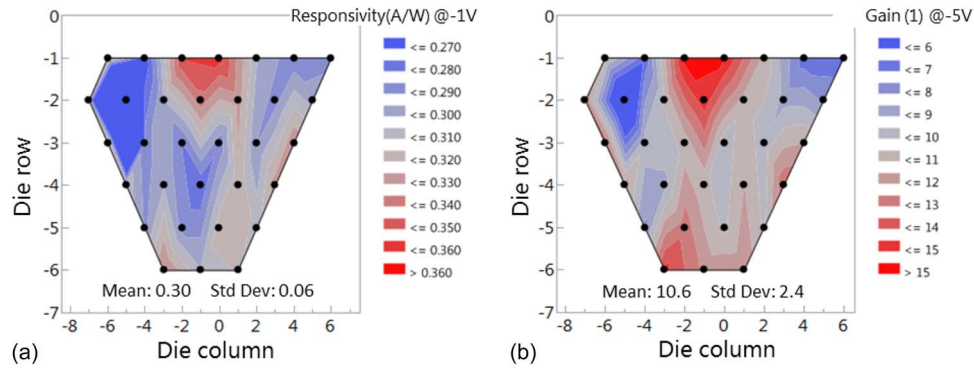


Fig. 4. (a) Wafer-scale primary responsivity data (at  $-1$  V) under an input optical power of  $-19.8$  dBm. (b) Wafer-scale avalanche gain data extracted from static measurements at  $-5$  V under an input optical power of  $-19.8$  dBm.

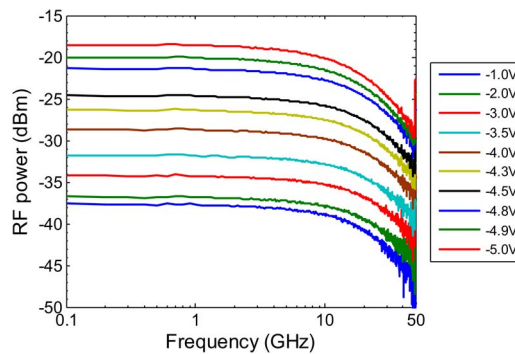


Fig. 5. Small-signal RF measurements of the  $S_{21}$  parameter for various bias voltages under an input optical power of  $-14.2$  dBm. The  $S_{21}$  parameter rises significantly with increasing bias voltage.

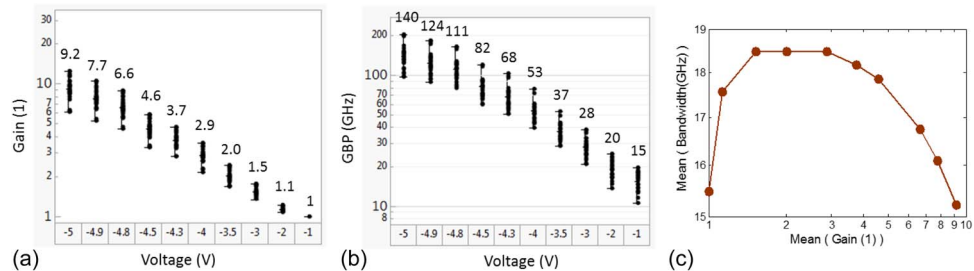


Fig. 6. (a) Wafer-scale avalanche gain data extracted from small-signal RF measurements for various bias voltages. (b) Wafer-scale gain  $\times$  bandwidth product (GBP) data. (c) Mean value of measured 3-dB opto-electrical bandwidth data (at a given reverse bias) versus the mean value of avalanche gain data (at the same reverse bias) extracted from small-signal measurements.

avalanche gain data extracted from these small-signal measurements. It reaches a mean value of 9.2 at  $-5$  V. The wafer-scale gain  $\times$  bandwidth product (GBP) data is shown in Fig. 6(b). The mean value is 140 GHz at  $-5$  V. Fig. 6(c) shows the mean value of the 3-dB bandwidth data (at a given reverse bias) as a function of the mean value of avalanche gain data (at that same reverse bias). The increase of the 3-dB bandwidth below an avalanche gain value of 2 is due to the widening of the depletion region in the Ge layer. As the gain gets larger than 4, the 3-dB bandwidth drops quickly due to the avalanche build-up time.

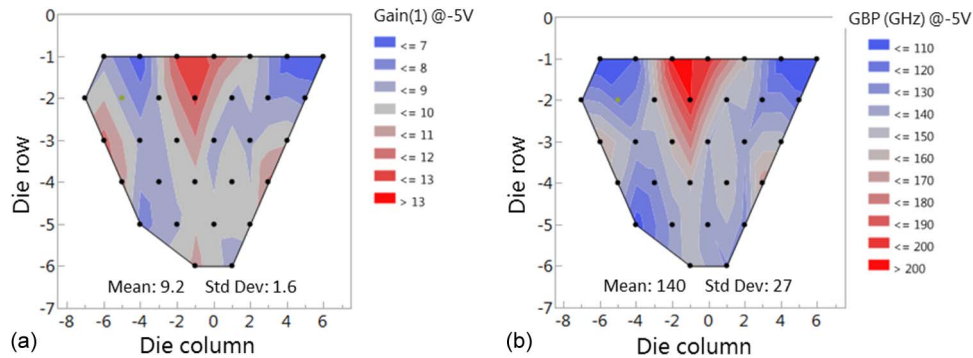


Fig. 7. (a) Contour plot of the wafer-scale avalanche gain data at  $-5$  V bias, as shown in Fig. 6(a). (b) Contour plot of the wafer-scale gain $\times$ bandwidth product data at  $-5$  V bias, as shown in Fig. 6(b).

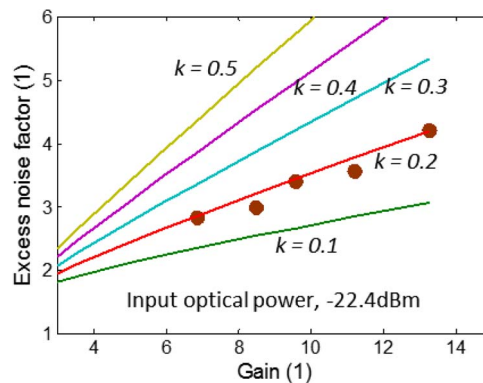


Fig. 8. Excess noise factor as a function of avalanche gain for an input optical power of  $-22.4$  dBm.

A contour plot of wafer scale avalanche gain data of the Ge APD at  $-5$  V bias is shown in Fig. 7(a). The mean avalanche gain value is 9.2 with a standard deviation of 1.6. The similar magnitude and pattern of the wafer-scale avalanche gain data extracted from static measurements and small-signal measurements confirm the validity of the avalanche gain definition in both types of measurements. Fig. 7(b) shows the contour plot of wafer scale GBP data at  $-5$  V bias. The mean value is 140 with a standard deviation of 27.

### 3.3. Avalanche Excess Noise Characteristics

Next, multiplication noise measurements were performed to characterize the avalanche multiplication noise. The noise current power spectral density (PSD) at 250 MHz in both dark current and light current (at 1310 nm wavelength) was measured using a low-noise signal analyzer. The excess noise factor  $F(M)$  as a function of gain is shown in Fig. 8 for an input optical power of  $-22.4$  dBm. The excess noise factor can be expressed for the case of avalanche multiplication in a uniform electric field with electrons initiating the multiplication as

$$F(M) = k_{\text{eff}}M + (2 - 1/M) \times (1 - k_{\text{eff}}) \quad (1)$$

where  $k_{\text{eff}}$  is the effective ratio of ionization coefficients for holes and electrons. Fitting the data with (1) reveals a  $k_{\text{eff}}$  of 0.2 in the presented device. Such a low value (the  $k$ -value is close to 1 in bulk germanium) is a signature of multiplication noise suppression owing to the thin avalanche multiplication region [3], [7]–[9].

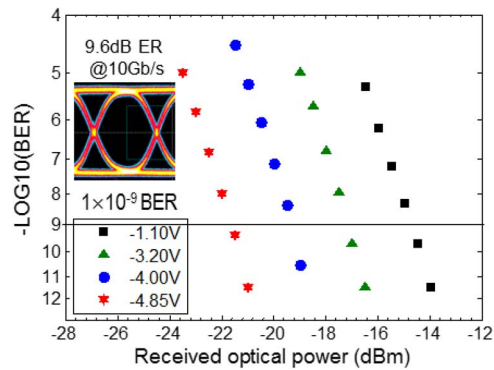


Fig. 9. Measured BER at 10 Gbps as a function of input optical power for various bias voltages using a  $(2^{31} - 1)$  long optical NRZ PRBS pattern at 1310 nm. The inset is the 10 Gbps input eye generated by a commercial optical modulator with an extinction ratio of 9.6 dB.

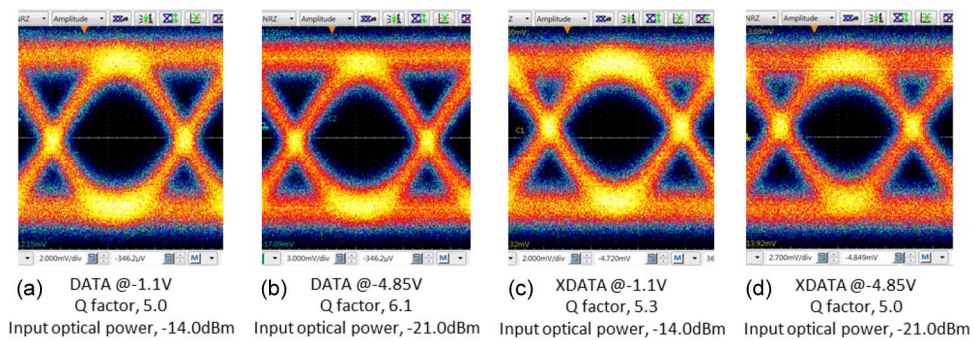


Fig. 10. A 10 Gbps eye diagrams of the electrical signal with a BER of  $3 \times 10^{-12}$  from (a) TIA DATA port at  $-1.1$  V APD bias, (b) TIA DATA port at  $-4.85$  V APD bias, (c) TIA XDATA port at  $-1.1$  V APD bias, and (d) TIA XDATA port at  $-4.85$  V APD bias, respectively.

## 4. APD Receiver Characteristics

### 4.1. 10 Gbps APD Receiver Sensitivity Measurements

A 10 Gbps optical receiver was constructed by wire-bonding an APD device to a 10 Gbps trans-impedance amplifier (TIA) to assess the receiver sensitivity. The 10 Gbps TIA [10], [11] used is the same as that adopted in [5], and has an input referred root-mean-square (RMS) noise current lower than  $1.2 \mu\text{A}$ . A  $(2^{31} - 1)$  long non-return-to-zero (NRZ) pseudo-random bit sequence (PRBS) data pattern at 10 Gbps, generated by a commercial optical modulator with 9.6 dB extinction ratio at 1310 nm wavelength (as shown in the inset of Fig. 9), was launched into the wire-bonded APD receiver. The measured bit error ratio (BER) as a function of input optical power for various bias voltages is shown in Fig. 9. For a BER of  $1 \times 10^9$ , the waveguide-referred primary sensitivity is  $-14.7$  dBm average optical power at  $-1.1$  V bias voltage. A 7 dB sensitivity improvement is obtained at  $-4.85$  V bias voltage, yielding an absolute receiver sensitivity of  $-21.7$  dBm for a  $1 \times 10^9$  BER. The avalanche gain, extracted from small-signal measurements, is larger than 7 at  $-4.85$  V bias. The higher sensitivity improvement of 7 dB at a larger gain of  $> 7$  compared to that reported in [5] results from the lower effective  $k$ -value of 0.2 than that of 0.5 reported in [5] by adopting an 185 nm thin Ge layer. 10 Gbps eye diagrams of the electrical signals from the TIA at a BER of  $3 \times 10^{-12}$  at both  $-1.1$  V and  $-4.85$  V bias voltages from both the DATA and XDATA port were recorded by a high-speed oscilloscope, as shown in Fig. 10.

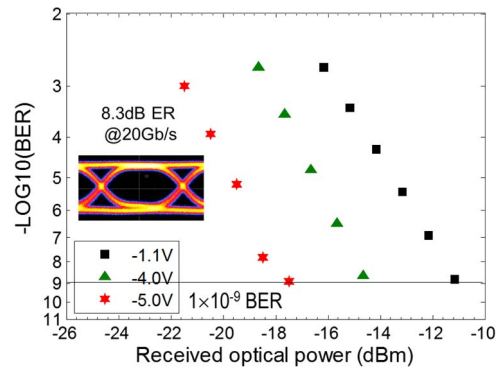


Fig. 11. BER at 20 Gbps as a function of input optical power using a  $(2^{31} - 1)$  long NRZ PRBS pattern at 1310 nm. (Inset) shows the 20 Gbps optical input eye diagram with an extinction ratio of 8.3 dB.

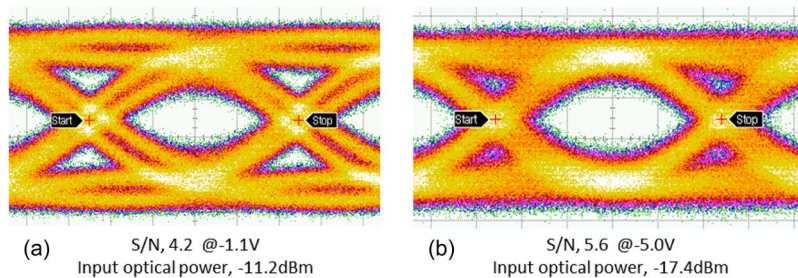


Fig. 12. Twenty Gbps eye diagrams of the electrical signal with a BER of  $2 \times 10^{-9}$  from TIA at  $-1.1$  V and (b) at  $-5.0$  V APD bias, respectively.

#### 4.2. 25 Gbps APD Receiver Sensitivity Measurements

A higher data-rate optical receiver is also built by wire-bonding another APD device to a 40 Gbps TIA. The  $0.13 \mu\text{m}$  SiGe BiCMOS TIA has an input referred (RMS) noise current of  $\sim 2 \mu\text{A}$  for 25 Gbps settings [12]. Fig. 11 shows the measured BER at 20 Gbps as a function of input optical power at 1310 nm wavelength. The waveguide-referred primary sensitivity is  $-11.2$  dBm average optical power at  $-1.1$  V bias voltage for a BER of  $1 \times 10^{-9}$ . A 6.2 dB sensitivity improvement is obtained at  $-5.0$  V bias voltage, yielding an absolute receiver sensitivity of  $-17.4$  dBm for a  $1 \times 10^{-9}$  BER. The avalanche gain, extracted from small-signal measurements, is  $\sim 9$  at  $-5.0$  V bias. The inset of Fig. 11 shows an eye diagram of the 20 Gbps optical NRZ PRBS data pattern ( $(2^{31} - 1)$  long) with 8.3 dB extinction ratio at 1310 nm wavelength used for the BER measurements. The 20 Gbps eye diagrams of the electrical signal from the TIA with a BER of  $2 \times 10^{-9}$  at both  $-1.1$  V and  $-5.0$  V bias voltage is shown in Fig. 12(a) and (b), respectively.

Operation at 25 Gbps was also evaluated. The obtained BER at  $-5$  V APD bias at 25 Gb/s for the wire-bonded optical receiver is shown in Fig. 13. The absolute sensitivity is  $-14.8$  dBm for a  $1 \times 10^{-9}$  BER. A 25 Gbps eye diagram of the electrical signal from the TIA with a BER of  $2 \times 10^{-9}$  at  $-5.0$  V APD bias is shown in the inset of Fig. 13, where eye degradation owing to the APD bandwidth limitation starts to be observed. The 2.6 dB power penalty for a  $1 \times 10^{-9}$  BER at 25 Gbps compared to that at 20 Gbps can be largely attributed to this bandwidth limitation (15.2 GHz) of the APD at  $-5.0$  V bias voltage.

## 5. Discussion

In the presented device, the low primary responsivity of 0.3 A/W is a limiting factor for further improving the sensitivity of the APD based optical receiver. There are four potential factors

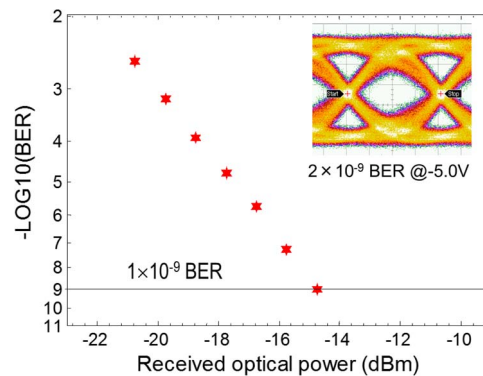


Fig. 13. BER at 25 Gbps using a  $(2^{31} - 1)$  long NRZ PRBS pattern at 1310 nm at  $-5.0$  V APD bias. (Inset) 25 Gbps eye diagram of the electrical signal with a BER of  $2 \times 10^{-9}$  from TIA at  $-5.0$  V APD bias.

responsible for the low primary responsivity: light absorption from the tungsten via contacts, free-carrier absorption, (valence) band-filling induced Ge absorption reduction, and a low photo-carrier collection efficiency. Optimizing the taper design to confine the incoming lightwave from the Si waveguide to the middle of the Ge layer is an effective way to minimize the light absorption from via contacts. Adopting a dotted ion implant window layout rather than a continuous implant window layout (as adopted in this paper) will effectively reduce both free-carrier absorption and Ge absorption reduction due to the Boron doping induced valence band filling. At the same time, it also increases the photo-carrier collection efficiency.

## 6. Conclusion

Waveguide-coupled Ge APDs adopting an 185 nm thin Ge layer are demonstrated with a wafer-scale mean gain $\times$ bandwidth product value of 140 GHz at  $-5$  V bias. The wire-bonded 20 Gbps optical receiver based on such a Ge APD demonstrates a 6.2 dB avalanche sensitivity improvement at  $-5$  V APD bias. Operation at 25 Gbps is demonstrated as well. Such low voltage Ge APDs allow lowering the power budget of silicon photonics optical interconnects.

## Acknowledgment

The authors acknowledge the process line at IMEC for manufacturing the Ge APD devices. They also thank D. Frederickx and L. Viaene for the wire bonding of the Ge APDs to TIAs.

## References

- [1] J. C. Campbell, "Recent advances in telecommunications avalanche photodiodes," *J. Lightw. Technol.*, vol. 25, no. 1, pp. 109–121 Jan. 2007.
- [2] Y. Kang *et al.*, "Monolithic germanium/silicon avalanche photodiodes with 340 GHz gain-bandwidth product," *Nat. Photon.*, vol. 3, no. 1, pp. 59–63, 2009.
- [3] S. Assefa, F. Xia, and Y. A. Vlasov, "Reinventing germanium avalanche photodetector for nanophotonic on-chip optical interconnects," *Nature*, vol. 464, no. 7285, pp. 80–84, 2010.
- [4] M. Nada, T. Yoshimatsu, Y. Muramoto, H. Yokoyama, and H. Matsuzaki, "Design and performance of high-speed avalanche photodiodes for 100-Gb/s systems and beyond," *J. Lightw. Technol.*, vol. 33, no. 5, pp. 984–990, Mar. 2015.
- [5] H. T. Chen *et al.*, "High sensitivity 10 Gb/s Si photonic receiver based on a low-voltage waveguide-coupled Ge avalanche photodetector," *Opt. Exp.*, vol. 23, no. 2, pp. 815–822, Jan. 2015.
- [6] P. Verheyen *et al.*, "Highly uniform 25 Gb/s Si photonics platform for high-density, low-power WDM optical interconnects," presented at the Advanced Photon. Commun. Opt. Soc. Amer. Conf., 2014, paper IW3A.4.
- [7] M. M. Hayat, B. E. A. Saleh, and M. C. Teich, "Effect of dead space on gain and noise of double-carrier multiplication avalanche photodiodes," *Trans. Electron Devices*, vol. 39, no. 3, pp. 546–552, Mar. 1992.
- [8] M. M. Hayat *et al.*, "Boundary effects on multiplication noise in thin heterostructure avalanche photodiodes: Theory and experiment," *Trans. Electron Devices*, vol. 49, no. 12, pp. 2114–2123, Dec. 2002.

- [9] S. C. Liew, C. H. Tan, Y. L. Goh, A. R. Marshall, and J. P. R. David, "Modeling of avalanche multiplication and excess noise factor in InAlAs avalanche photodiodes using a simple Monte Carlo model," *J. Appl. Phys.*, vol. 104, no. 1, 2008, Art. ID. 013114.
- [10] X. Yin *et al.*, "Experiments on 10 Gb/s fast settling high sensitivity burst-mode receiver with on-chip auto-reset for 10 G-GPONs [Invited]," *IEEE/OSA J. Opt. Commun. Netw.*, vol. 4, no. 11, B68–B76, Nov. 2012.
- [11] X. Yin *et al.*, "A 10 Gb/s burst-mode TIA with on-chip reset/lock CM signaling detection and limiting amplifier with a 75 ns settling time," in *IEEE ISSCC Dig. Tech. Papers.*, Feb. 2012, pp. 416–417.
- [12] B. Moeneclaey *et al.*, "A 40 Gb/s transimpedance amplifier for optical links", *IEEE Photon. Technol. Lett.*, vol. 27, no. 13, pp. 1375–1378, Jul. 2015.